ADVANCED FUNCTIONAL MATERIALS

Supporting Information

for *Adv. Funct. Mater.*, DOI: 10.1002/adfm.201302405

Self-Assembly Mechanism of Spiky Magnetoplasmonic Supraparticles

Hongjian Zhou, Jong-Pil Kim, Joong Hwan Bahng, Nicholas A. Kotov, and Jaebeom Lee**

Submitted to ADVANCED FUNCTIONAL MATERIALS

Supporting Information

for *Adv. Funct. Mater.*, DOI: 10.1002/adfm. 201302405

Self-Assembly Mechanism of Spiky Plasmonic Supraparticles

Hongjian Zhou, Jong-Pil Kim, Joong Hwan Bahng, Nicholas A. Kotov*, Jaebeom Lee*

Additional Methods:

Absorbance of the Fe_3O_4@Au SPs was measured by UV-vis spectroscopy (S310, SCINCO, Korea) using 1cm quartz cuvettes and deionized water as the background. The morphologies and sizes of the nanoparticles were characterized using HR-TEM (JEM-3010, JEOL, Japan) operating at 200 kV. The TEM grid preparation was as follows. A drop of the Fe_3O_4@Au SPs solution was placed on a TEM grid using a pipette. The TEM grid was a 400-mesh carbon-coated copper grid (Electron Microcopy Sciences). The drop on the grid was allowed to dry under open atmosphere. The Fe_3O_4@Au SPs were then examined with TEM and EDS. Their surface potentials and particle size distribution were determined by a zeta-sizer (Nano ZS, Malvern Instruments, Great Britain) using 1cm quartz cuvettes. An X-ray powder diffractometer (D8 FOCUS 2.2 kW, Bruker, Germany) was used to characterize the Fe_3O_4@Au SPs with Cu Ka radiation and a Ni filter. To prepare samples for XRD, 5 mg of the Fe_3O_4@Au SPs was dried in a vacuum oven at ambient temperature. The dried SP powder was pressed onto one side of double-sided Scotch tape on a piece of glass slide. The data were collected at 2θ from 10° to 90° at a scan rate of 0.06° per step and 2 s per point.

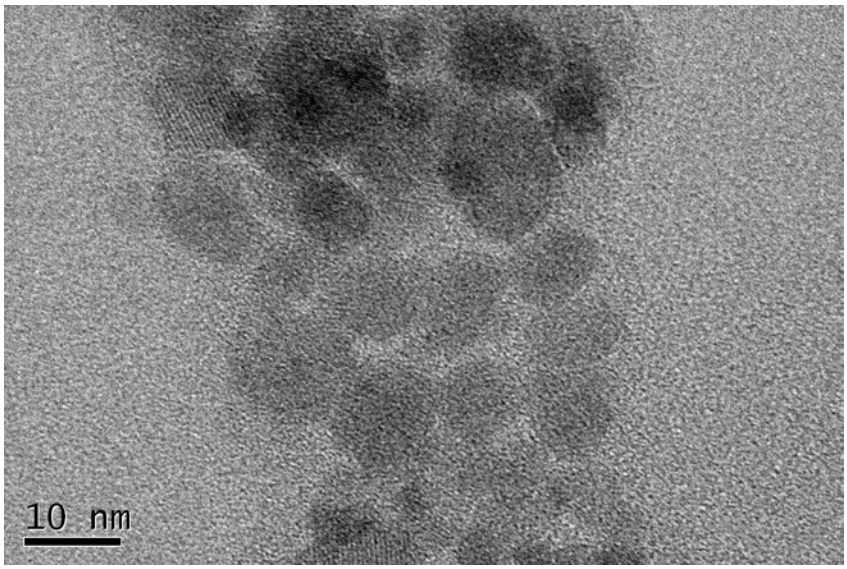

Figure S1. High magnification TEM image of Fe_3O_4 NPs

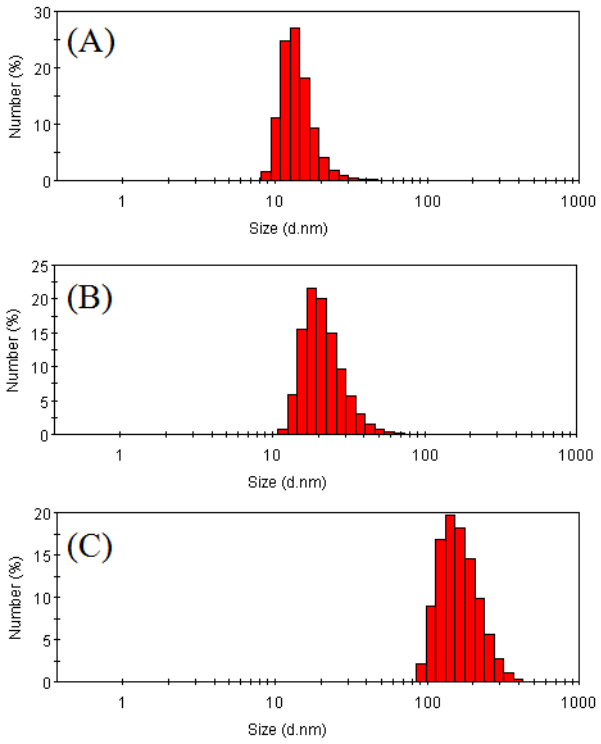

Figure S2. Size distribution of (A) Fe_3O_4 NPs; (B) spherical Fe_3O_4@Au core-shell particles; (C) spiky SPs.

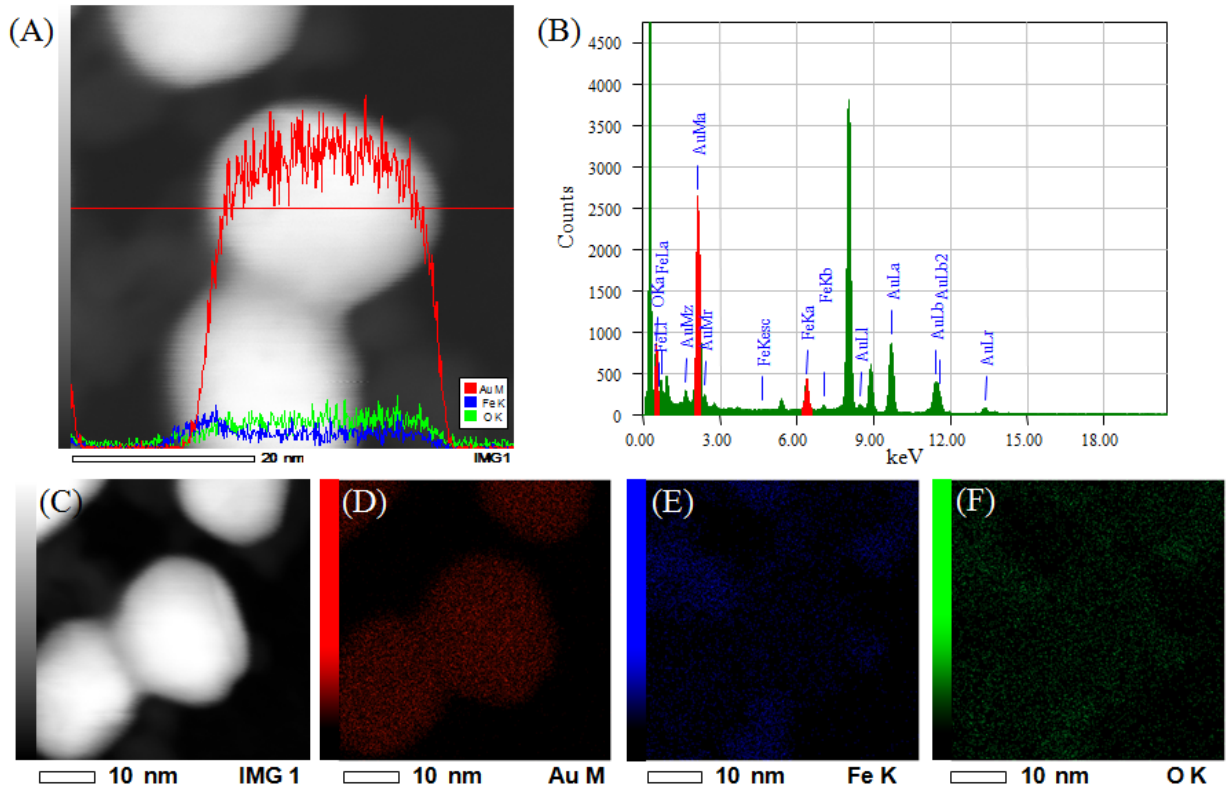

Figure S3. (A) TEM micrograph and line map curve of Fe_3O_4@Au NPs in dark field; (B) EDX spectra of the selected scan area; (C) the whole area mapping analysis of nanoparticles in dark field showing the distribution of (D) Fe, (E) Au and (F) O in synthesized nanoparticles. Red, green and blue dots represent Fe, Au and O, in (D), (E), and (F), respectively.

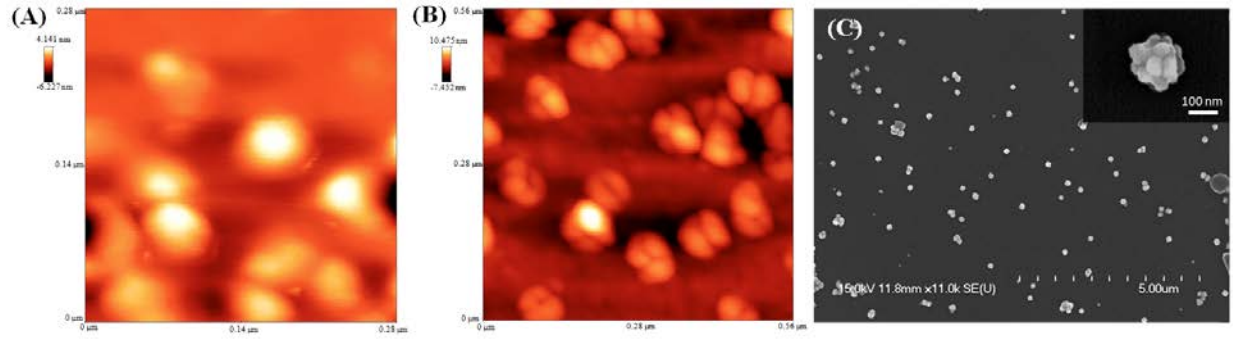

Figure S4. AFM images of (A) spherical Fe_3O_4@Au seed NPs and (B) spiky Fe_3O_4@Au core-shell SPs; (C) SEM image of spiky Fe_3O_4@Au core-shell SPs

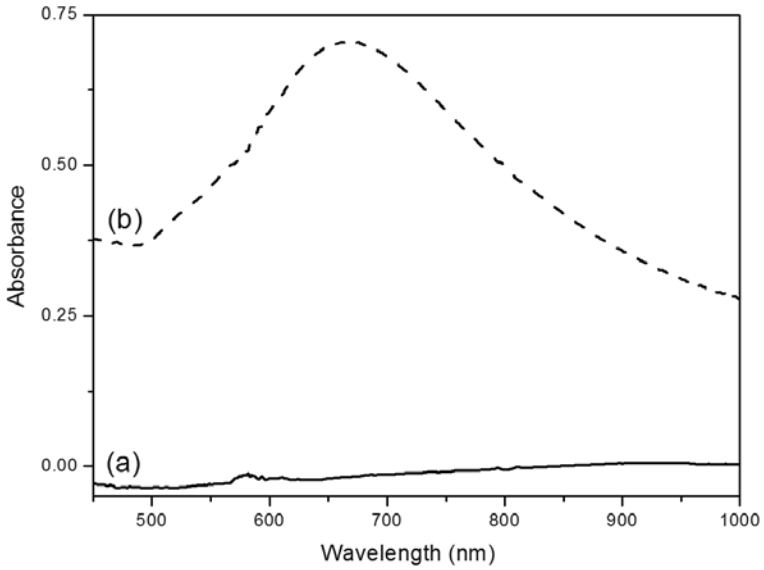

Figure S5. UV-vis spectra of the hydroquinone-mediated reduction of $HAuCl_4$ in the (a) absence, and (b) presence of Fe_3O_4@Au core−shell particle seeds.

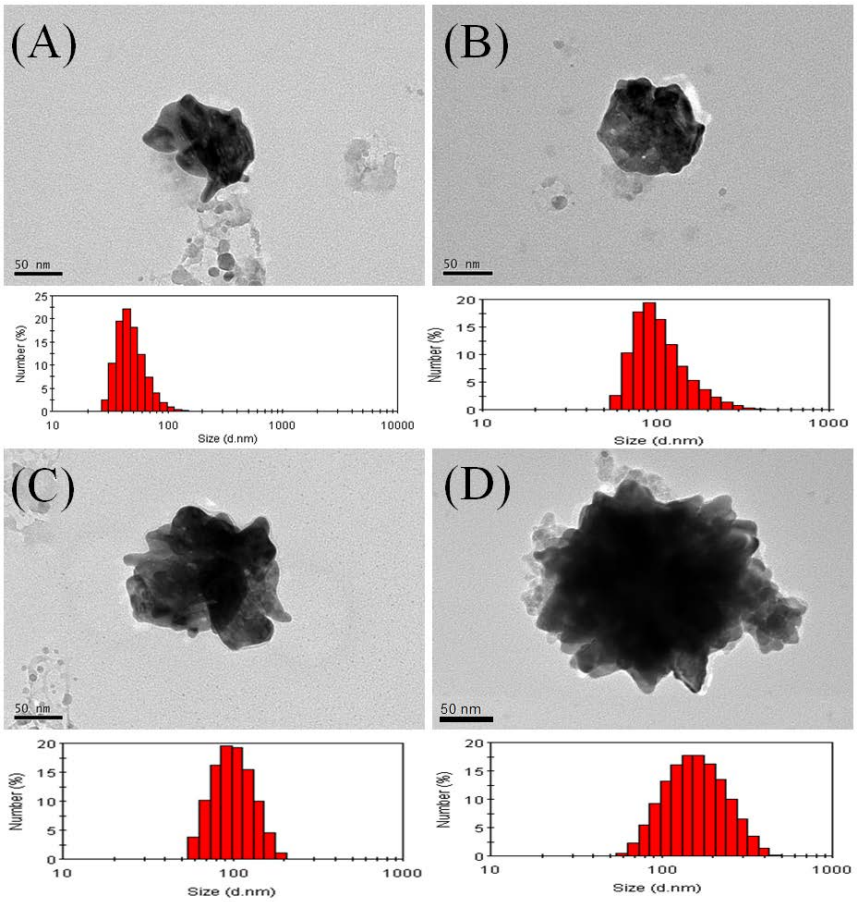

Figure S6. TEM images and size distribution curves of spiky SPs during growth. (A) 5 min; (B) 10 min; (C) 15 min and (D) 20 min.

Preparation of one-dimensional alignment of Fe_3O_4@Au NPs

The one-dimensional (1-D) alignment of *magnetoplasmonic nanowires* (MPNWs) was obtained via external magnetic force using commercial neodymium (NdFeB) blocks magnets (1.8 T) in the solution state (**Figure S7−A**). Approximately 14 µL of Fe_3O_4@Au NPs (6 µg/ml) was dropped onto the glass substrate (electrode) located above the interface of two block magnets at a distance of 10 mm. The setup was put in an oven at 40 ^{o}C and left until water was completely evaporated.

The electrodes were characterized in terms of linear sweep voltammetry using IviumStat (Ivium Technologies, The Netherlands) in a dry state. The voltage was swept from −100 to +100 mV with steps of 5 mV and the current was recorded. The slope of the current–voltage (I–V) plot was calculated using linear regression analysis and the inverse of this value, the resistance (R), was used for comparison purposes.

Because of the multifunctional (magnetic, optical and conductive) properties of the Au-coated iron oxide core−shell NPs, we simply made one dimensional of these NPs with more than 100 µm in length and 100-200 nm in diameter are bridged over microelectrode under external magnetic field (as shown in **Figure S7**). **Figure S7−C and D** show the morphology and magnetic properties of MPNWs on the substrate. The MPNWs bridged over an electrode area of 50 × 50 µm. A magnetic force microscopy (MFM) image of the same area is shown in **Figure S7−D**. The probe was magnetized in the direction perpendicular to the substrate and the lift height was 300 nm. It has been reported that the magnetic field-induced alignment of superparamagnetic nanoparticles shows ferromagnetic behavior at room temperature. Hence, the clear stray field observed in the MFM image is the result of magnetostatic interaction between the MPNWs. Moreover, the MPNWs that formed a bridge over the microelectrode have conductivity, as shown in **Figure S7−E**. Therefore, according to the current results, we can infer that the Fe_3O_4@Au NPs are Au coated iron oxide core−shell NPs.

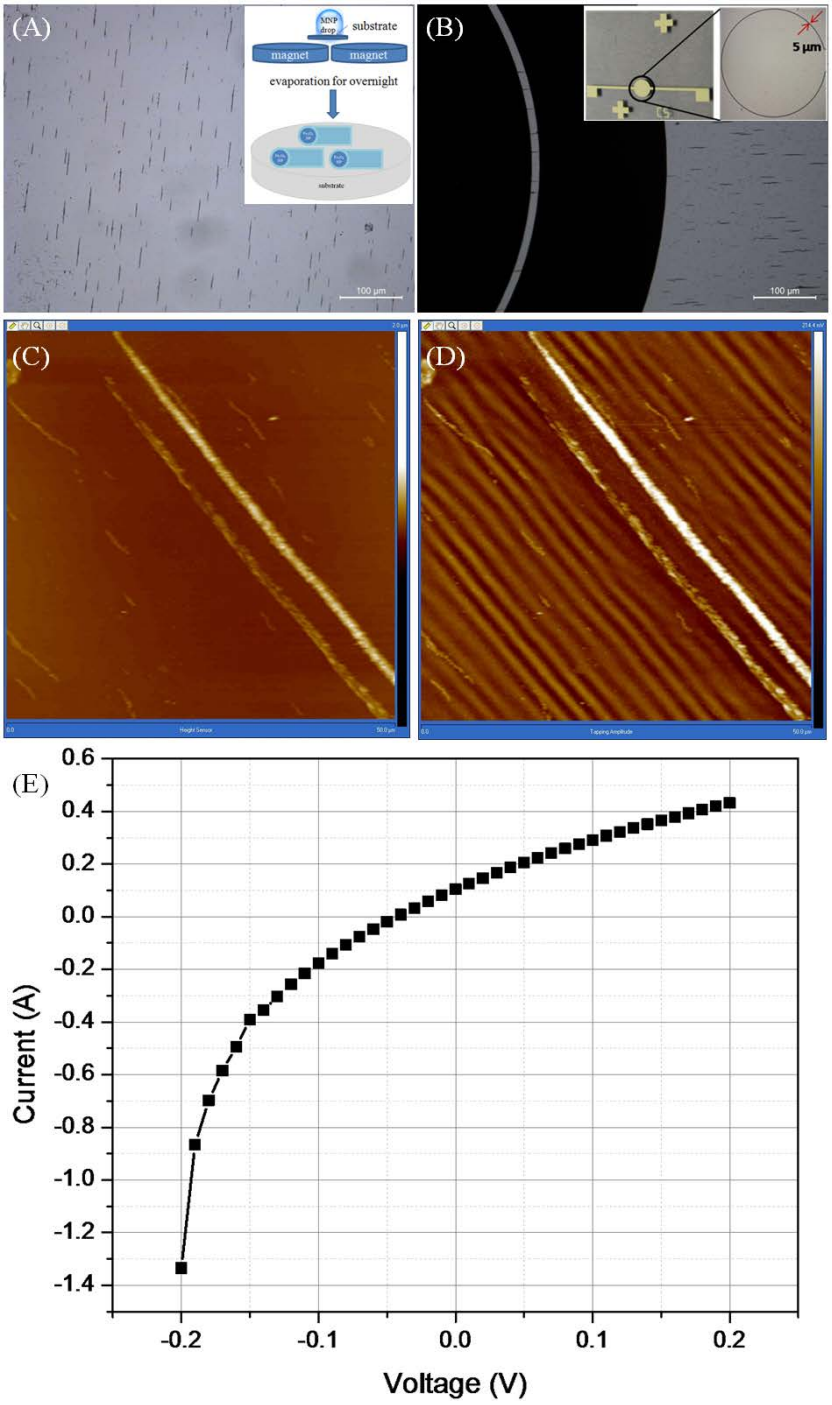

Figure S7. (A) Optical microscopic images of MPNWs prepared from Fe_3O_4@Au solutions; (B) MPNWs bridge over circular electrode; (C) AFM image and (D) magnetic force microscope (MFM) image of MPNWs in small area; (E) *I–V curves of* MPNW bridge over circular electrode.

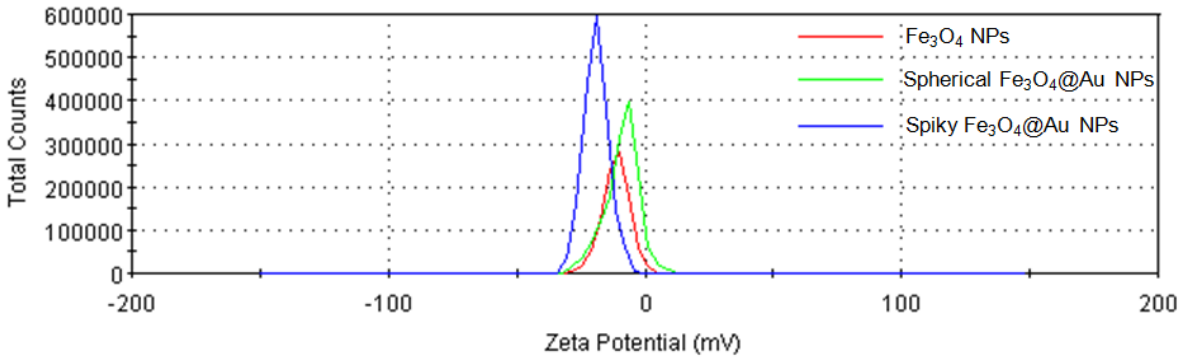

Figure S8. Zeta potential of Fe_3O_4 NPs (red line); spherical Fe_3O_4@Au seed NPs (green line) and spiky Fe_3O_4@Au core-shell SPs (blue line).

Interaction potential between hydroquinone reduced Au NPs and the Fe_3O_4@Au SPs at various stages

***Stage i*, Potential between Fe_3O_4@Au core–shell and *hydroquinone* reduced gold NP;**

Assumption: Interaction between spherical Au NP_2 and hydroquinone reduced gold spherical NP_1

Specifications: $R_1 = 5nm$, $R_2 = 12.5nm$, $A_{131} = 2.5 \times 10^{-19} J$,[1] $\zeta_1 = -9.77\ mV$, $\zeta_2 = -8.97\ mV$

***Stage g*, Potential between intermediate SP and** hydroquinone **reduced gold NP;**

Assumption: Interaction between spherical Au NP_3 and hydroquinone reduced gold spherical NP_1

Specifications: $R_1 = 5\text{nm}$, $R_3 = 50\text{nm}$, $A_{131,\text{eff}} = 1.41 \times 10^{-19}\text{J}$, $\zeta_1 = -9.77\ \text{mV}$, $\zeta_3 = -19.1\ \text{mV}$. The effective Hamaker's constant, $A_{131,\text{eff}}$, is calculated with the assumption that the shell is a composite of water and gold using the following expression,[2]

$$A_{131,eff} = \left[V_{Au}(A_{131})^{\frac{1}{2}} + (1 - V_{Au})(A_{133})^{\frac{1}{2}}\right]^2$$

$$= {V_{Au}}^2 A_{131}$$

, where V_{Au}, the volume fraction of Au, is assumed to be 75% of the total SP volume at this growth stage.

Stage f, **Potential between fully grown SP and** hydroquinone **reduced gold NP;**

Assumption: Interaction between spherical Au NP_4 and hydroquinone reduced gold spherical NP_1

Specifications: $R_1 = 5nm$, $R_4 = 92.5nm$, $\zeta_1 = -9.77$ mV, $\zeta_4 = -19.1$ mV. Here, $V_{Au} =$ 25.6% (assuming each spike is a cone whose length and height is determined from TEM) which yields $A_{131,eff} = 1.645 \times 10^{-19} J$.

Stage 0, **Potential between bare Fe_3O_4 NP and** hydroquinone **reduced gold NP;**

Specifications: $R_1 = 5nm$, $R_5 = 5nm$, $\zeta_1 = -9.77$ mV (REF), $\zeta_4 = -19.1$ mV. Hamaker's constant of interaction between Fe_3O_4 and Au across water, A_{132}, is obtained from the following expression[3]

$$A_{132} = \left(\sqrt{A_{11}} - \sqrt{A_{33}}\right)\left(\sqrt{A_{22}} - \sqrt{A_{33}}\right)$$

, where $A_{11} = 4.53 \times 10^{-19}$ J, $A_{22} = 2.1 \times 10^{-19}$ J, $A_{33} = 3.7 \times 10^{-20}$ J,[4] which yields $A_{132} = 1.03 \times 10^{-19}$J.

Reference List

[1] S.Biggs, P.Mulvaney, *The Journal of Chemical Physics* **1994**, *100*, 8501.

[2] B.Vincent, *Journal of Colloid and Interface Science* **1973**, *42*, 270.

[3] J.N.Israelachvili, *Intermolecular and surface forces: revised third edition*, Academic press, **2011**.

[4] J.Goodwin, *Colloids and interfaces with surfactants and polymers*, Wiley, **2009**.